Decentralized Feedback Maneuver of Flexible Spacecraft

Larry Silverberg* and Lester A. Foster†
North Carolina State University, Raleigh, North Carolina

This paper describes a novel approach to flexible spacecraft maneuver in which spacecraft motion relative to the motion of a shadow spacecraft is suppressed using a decentralized feedback control. The shadow spacecraft is a fictitious spacecraft that can be positioned, oriented, and allowed to undergo elastic deformations at the discretion of the designer. First, rest-to-spin maneuvers are investigated, with different choices for the shadow coordinates. The angular velocities of the shadow coordinates are chosen as step functions, quadratic functions corresponding to minimum fuel maneuvers for rigid bodies, and quadratic functions with lag compensation in which the lag is associated with the spacecraft angular velocities relative to the shadow spacecraft angular velocities. The performance of the maneuvers is illustrated in the presence of multiple actuator failures. Next, both in-plane and out-of-plane rest-to-rest maneuvers are investigated. The associated shadow coordinates are chosen to correspond to those of minimum fuel maneuvers and minimum fuel maneuvers with lag compensation.

I. Introduction

THE problem of maneuvering flexible spacecraft has traditionally been cast in the form of nonlinear two-point boundary-value problems. Although solutions to the general nonlinear two-point boundary-value problem can be obtained for rigid spacecraft, the computational effort and the numerical sensitivities can often pose problems.[1] For flexible spacecraft, the solution of the nonlinear two-point boundary-value problem may be close to unattainable in the extreme case and, at the very least, provides little insight into algorithms well suited for in-space implementation. This paper describes a novel approach to the problem of maneuvering flexible spacecraft in which spacecraft motion relative to the motion of a shadow spacecraft is suppressed using a decentralized feedback control. The shadow spacecraft is a fictitious spacecraft whose motion is freely prescribed by the designer. Thus, the shadow spacecraft may be positioned and oriented and may undergo flexible-body motions if so desired. An inherent level of system level reliability is then obtained by suppressing motion relative to the shadow spacecraft using decentralized feedback.[2]

In Sec. II, the dynamics of a nondimensional free-free beam with well-separated dimensions are described, and a general formulation for the associated control law is given. This representative spacecraft will be used throughout the remainder of the paper. In Sec. III, we investigate decentralized feedback spin-up maneuvers with different choices for the shadow spacecraft. Decentralized feedback rest-to-rest maneuvers are then considered in Sec. IV.

II. Maneuver of a Free-Free Beam with Well-Separated Dimensions

Consider the free-free uniform beam of length l, width w, and cross-sectional thickness c, with well-separated dimensions so that $c \ll w \ll l$. The beam undergoes bending vibration in the $\hat{b}_2$ direction (see Fig. 1), and so the stiffness operator for the beam has the form $L = EI\partial^4/\partial x^4 \hat{b}_2\hat{b}_2$, where EI denotes the bending stiffness of the beam.[3] The mass per unit length of the beam is denoted by ρ, with $M = \rho L$ representing the total mass of the beam and $I_1 = (M/12)(w^2 + c^2)$, $I_2 = (M/12)(w^2 + l^2)$, and $I_3 = (M/12)(c^2 + l^2)$ representing the principal mass moments of inertia of the beam about the three axes of the floating coordinates, respectively.[4] The inertial position of any point on the spacecraft is expressed as

$$u = u_0 + u_C + u_E \tag{1}$$

with

$$u_0 = u_0(t) = u_{01}(t)\hat{i}_1 + u_{02}(t)\hat{i}_2 + u_{03}(t)\hat{i}_3$$

which is the position of the beam's mass center (coinciding with the origin of the floating coordinates) measured in inertial coordinates with unit vectors $\hat{i}_1$, $\hat{i}_2$, and $\hat{i}_3$, and

$$u_C = u_C(P,t) = x_1\hat{b}_1(t) + x_2\hat{b}_2 + x_3\hat{b}_3$$

which is the nominal position to point P relative to the mass center of the beam measured in floating coordinates with unit vectors $\hat{b}_1(t)$, $\hat{b}_2(t)$, and $\hat{b}_3(t)$ (see Fig. 2).

In the case of our free-free beam, $u_C(P) = x\hat{b}_2$. The elastic displacement is orthogonal to the rigid-body modes of vibration and expressed as a linear combination of elastic modes of vibration measured relative to the floating coordinates as[5]

$$u_E = \sum_{r=1}^{\infty} \phi_{Er} q_r \tag{2}$$

with $u_E = u_E(P,t) = u_{E1}(P,t)\hat{b}_1 + u_{E2}(P,t)\hat{b}_2 + u_{E3}(P,t)\hat{b}_3$, the elastic displacement of the spacecraft; $\phi_{Er} = \phi_{Er}(P) = \phi_{Er1}(P)\hat{b}_1 + \phi_{Er2}(P)\hat{b}_2 + \phi_{Er3}(P)\hat{b}_3$, the rth elastic mode of

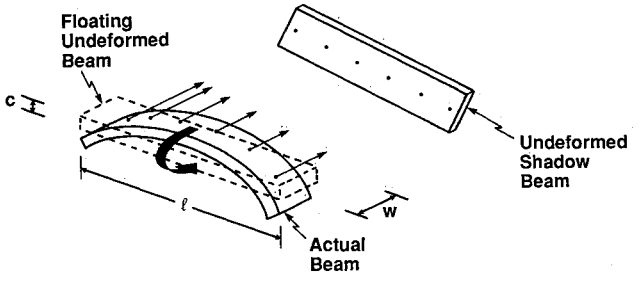

Fig. 1 Floating beam, actual beam, and shadow beam with six discrete control forces and one discrete control moment shown.

Received June 16, 1988; revision received Oct. 10, 1988.

*Assistant Professor, Mechanical and Aerospace Engineering.
†Graduate Research Assistant, Mechanical and Aerospace Engineering.

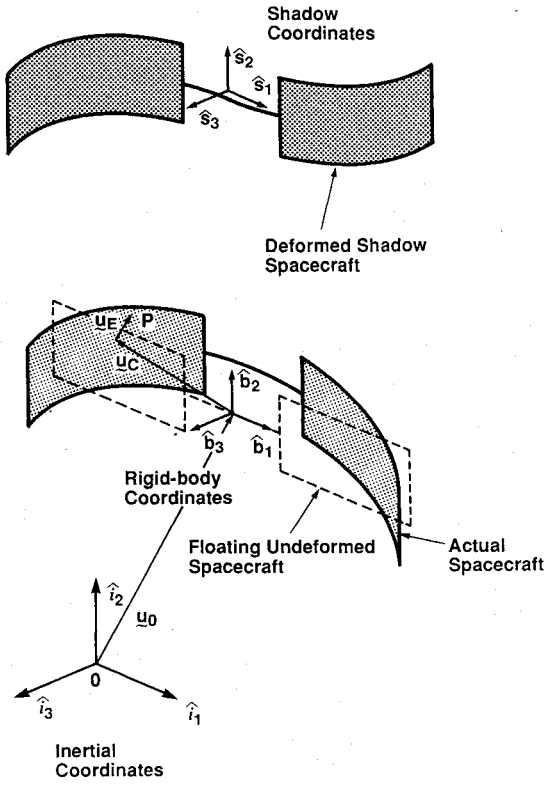

Fig. 2 Floating spacecraft, actual spacecraft, and shadow spacecraft with inertial position of point *P* shown.

vibration of the beam; and $q_r = q_r(t)$, the rth modal displacement.

In the case of our free-free beam, $\phi_{Er}(P) = \phi_{Er}(x)\hat{b}_2$, in which $\phi_{Er}(x)$ can be expressed in closed form.[3]

The translational, rotational, and modal equations of motion become

$$M\ddot{u}_{01} = F_1, \qquad M\ddot{u}_{02} = F_2, \qquad M\ddot{u}_{03} = F_3$$

$$I_1\dot{\Omega}_1 = (I_2 - I_3)\Omega_2\Omega_3 + M_1, \qquad I_2\dot{\Omega}_2 = (I_3 - I_1)\Omega_3\Omega_1 + M_2$$

$$I_3\dot{\Omega}_3 + (I_1 - I_2)\Omega_1\Omega_2 + M_3$$

$$\ddot{q}_r = -\omega_r^2 q_r + Q_r, \qquad (r = 1,2,\ldots) \tag{3}$$

where

$$F_2 = \int_{-l/2}^{l/2} f\,dx, \qquad Q_r = \int_{-l/2}^{l/2} \phi_{Er} f\,dx$$

with

$F = F(t) = F_1(t)\hat{i}_1 + F_2(t)\hat{i}_2 + F_3(t)\hat{i}_3$ (net external force vector acting on the beam)

$\Omega = \Omega(t) = \Omega_1(t)\hat{b}_1(t) + \Omega_2(t)\hat{b}_2(t) + \Omega_3(t)\hat{b}_3(t)$ (angular velocity vector of the floating coordinates)

$M = M(t) = M_1(t)\hat{b}_1(t) + M_2(t)\hat{b}_2(t) + M_3(t)\hat{b}_3(t)$ (net external moment vector acting on the beam)

$Q_r = Q_r(t)$ (rth modal control force)

$f = f(x,t)$ (control force distribution over the beam in the $\hat{b}_2$ direction)

and ω_r = the natural frequency of rth elastic mode of vibration of the beam.

The elastic modes of vibration are solutions to the eigenvalue problem

$$EI\frac{d^4\phi_{Er}}{dx^4} = \omega_r^2\rho\phi_{Er}, \qquad r = 1,2,\ldots \tag{4}$$

The decentralized feedback maneuvers considered in the next sections of this paper will be executed using six discrete control forces evenly spaced along the beam acting in the $\hat{b}_1$, $\hat{b}_2$, and $\hat{b}_3$ directions and using one discrete control moment at the center of the beam acting about the $\hat{b}_1$ axis (see Fig. 1). The components of the six discrete control forces acting in the $\hat{b}_2$ direction are expressed in terms of a distributed control force as

$$f = \sum_{r=1}^{6} f_{2r}\delta_r \tag{5}$$

with

$f_{ir} = f_{ir}(t)$, the rth discrete control force in $\hat{b}_i$ direction applied at x_r
$\delta_r = \delta(x - x_r)$, the spatial Dirac-delta function at x_r

The decentralized feedback maneuvers described in the next sections uniformly dampen the beam motion.[2] The beam motion is damped relative to a shadow beam specified in advance by the designer. The associated control law has the form

$$f_{ir} = -2\alpha m_r(\dot{u}_{ir} - \dot{u}_{sir}) - \alpha^2 m_r(u_{ir} - u_{sir}), \qquad r = 1,2,\ldots,6 \tag{6a}$$

$$M_1 = -2\alpha I_1(\dot{\theta}_1 - \dot{\theta}_{s1}) - \alpha^2 I_1(\theta_1 - \theta_{s1}) \tag{6b}$$

with

α = designer chosen uniform damping rate
m_r = beam mass in the subdomain of the rth control force
$u_{ir} = u_i(x_r,t)$, inertial position of point x_r in the $\hat{b}_i$ direction
$u_{sir} = u_{si}(x_r,t)$, inertial position of point x_r in the $\hat{b}_i$ direction of the shadow beam
$\theta_1 = \theta_1(t)$, angle of rotation of the beam about the $\hat{b}_1$ axis
$\theta_{s1} = \theta_{s1}(t)$, angle of rotation of the shadow beam about the $\hat{b}_1$ axis

in which overdots represent differentiations with respect to inertial space. From Eq. (6), the maneuver requires the selection of a uniform damping rate α and the selection of shadow coordinates. Issues regarding the selection of the uniform damping rate and the shadow coordinates will be treated in subsequent sections. The immediate interest lies in nondimensionalizing the problem according to

$$\bar{t} = t/T, \qquad \bar{x} = x/l, \qquad \bar{\Omega} = \Omega T \tag{7}$$

with

$\bar{t}$ = nondimensional time
$\bar{x}$ = nondimensional coordinate
$\bar{\Omega}$ = nondimensional angular velocity
$T = 2\pi(\rho L^4/EI)^{1/2}/\omega_f$, characteristic time constant (chosen identical to the fundamental period

Introducing Eqs. (7) into Eqs. (3-5), we obtain the nondimensional translational, rotational, and modal equations of motion, written explicitly as

$$\bar{u}_{01}'' = \bar{F}_1, \qquad \bar{u}_{02}'' = \bar{F}_2, \qquad \bar{u}_{03}'' = \bar{F}_3 \tag{8a}$$

$$\bar{\Omega}_1' = -\bar{\alpha}_1\bar{\Omega}_2\bar{\Omega}_3 + \bar{M}_1, \qquad \bar{\Omega}_2' = -\alpha_2\bar{\Omega}_3\bar{\Omega}_1 + \bar{M}_2$$

$$\bar{\Omega}_3' = -\bar{\alpha}_3\bar{\Omega}_1\bar{\Omega}_2 + \bar{M}_3 \tag{8b}$$

$$\bar{q}_r'' = -\bar{\omega}_r^2\bar{q}_r + \bar{Q}_r \tag{8c}$$

where

$$\bar{F}_2 = \int_{-\frac{1}{2}}^{\frac{1}{2}} \bar{f}\, d\bar{x} = \sum_{r=1}^{6} \bar{f}_{2r}, \qquad \bar{Q}_r = \int_{-\frac{1}{2}}^{\frac{1}{2}} \bar{\phi}_{Er} \bar{f}\, d\bar{x} \tag{9}$$

and we obtain the nondimensional eigenvalue problem

$$\frac{d^4 \bar{\phi}_{Er}}{d\bar{x}^4} = \bar{\omega}_r^2 \bar{\phi}_{Er} \tag{10}$$

in which primes represent derivatives with respect to nondimensional time with

$\bar{u}_{01} = u_{01}/l$, $\bar{u}_{02} = u_{02}/l$, $\bar{u}_{03} = u_{03}/l$ (nondimensional positions of beam mass center)

$\bar{F}_1 = F_1 T^2/Ml$, $\bar{F}_2 = F_2 T^2/Ml$, $\bar{F}_3 = F_3 T^2/Ml$ (nondimensional net external forces acting on the beam)

$\bar{M}_1 = M_1 T^2/I_1$, $\bar{M}_2 = M_2 T^2/I_2$, $\bar{M}_3 = M_3 T^2/I_3$ (nondimensional net external moment about the beam mass center)

$\bar{q}_r = q_r/M^{\frac{1}{2}}l$ (rth nondimensional modal displacement)

$\bar{f} = fT^2/M$ (nondimensional force per unit length of the beam)

$\bar{\phi}_{Er} = \phi_{Er} M^{\frac{1}{2}}$ (rth nondimensional natural mode of vibration)

$\bar{\omega}_r = \omega_r T$ [rth nondimensional natural frequency of oscillation (the fundamental nondimensional frequency $\bar{\omega}_f = \bar{\omega}_1 = 2\pi$)]

$\bar{f}_{ir} = f_{ir} T^2/Ml$ (rth nondimensional discrete control force in the $\hat{b}_i$ direction located at $\bar{x}_r = x_r/l$)

and with

$$\bar{\alpha}_1 = \frac{I_2 - I_3}{I_1} \approx 1, \quad \bar{\alpha}_2 = \frac{I_3 - I_1}{I_2} \approx 1, \quad \bar{\alpha}_3 = \frac{I_1 - I_2}{I_3} \approx -1$$

Finally, the nondimensional control law has the form

$$\bar{f}_{ir} = -2\bar{\alpha}\bar{m}_r(\bar{u}'_{ir} - \bar{u}'_{sir}) - \bar{\alpha}^2 \bar{m}_r(\bar{u}_{ir} - \bar{u}_{sir}) \tag{11a}$$

$$\bar{M}_1 = -2\bar{\alpha}(\theta'_1 - \theta'_{s1}) - \bar{\alpha}^2(\theta_1 - \theta_{s1}) \tag{11b}$$

with

$\bar{\alpha} = \alpha T$ (nondimensional designer chosen uniform decay rate)

$\bar{m}_r = m_r/M$ [nondimensional mass in the subdomain of the rth control force ($\bar{m}_1 = \bar{m}_6 = 0.1$, $\bar{m}_2 = \bar{m}_3 = \bar{m}_4 = \bar{m}_5 = 0.2$)]

$\bar{u}_{ir} = u_{ir}/l$ (nondimensional inertial position of point $\bar{x}_r = x_r/l$ in the $\hat{b}_i$ direction)

$\bar{u}_{sir} = u_{sir}/l$ (nondimensional inertial position of point $\bar{x}_r$ in the $\hat{b}_i$ direction on the shadow beam)

Throughout the remainder of the paper, the elastic motion of the beam is expressed as a linear combination of the 10 lowest natural modes of vibration. The contribution of the remaining modes to the overall system response is neglected.

III. Decentralized Feedback Spin-up Maneuvers

A. Angular Velocity of Shadow Coordinates Chosen as Step Function

As mentioned previously, decentralized feedback maneuver requires the selection of an appropriate shadow spacecraft relative to which spacecraft motion is suppressed. As a first illustration, consider shadow coordinates rotating about the principal axis $\hat{b}_3$ of the beam at an angular velocity in the form of the step function.

$$\bar{\Omega}_{s1}(\bar{t}) = 0, \quad \bar{\Omega}_{s2}(\bar{t}) = 0, \quad \bar{\Omega}_{s3}(\bar{t}) = \bar{\Omega}_m u(\bar{t}) \tag{12}$$

with

$\bar{\Omega}_m$ = nondimensional angular velocity of the shadow beam about $\hat{b}_3$

$u(\bar{t})$ = unit step function

In broad terms, the nondimensional angular velocity of the beam in the $\hat{b}_3$ direction, $\bar{\Omega}_3$, is expected to lag the nondimensional angular velocity of the shadow coordinates $\bar{\Omega}_{s3}$ increasingly as the nondimensional decay rate $\bar{\alpha}$ decreases. As a rule of thumb, $\bar{\alpha}$ must be chosen to be at least one-third the fundamental frequency of the beam. Otherwise, the control law does not allow the beam to "catch up" to the shadow beam. It follows that both the rise time and the settling time associated with $\bar{\Omega}_3$ decrease as $\bar{\alpha}$ increases, as shown in Fig. 3.

B. Angular Velocity of Shadow Coordinates Chosen as Optimal Profile

Previously, the angular velocity of the shadow coordinates were chosen in the form of a step function [Eqs. (12)]. In this

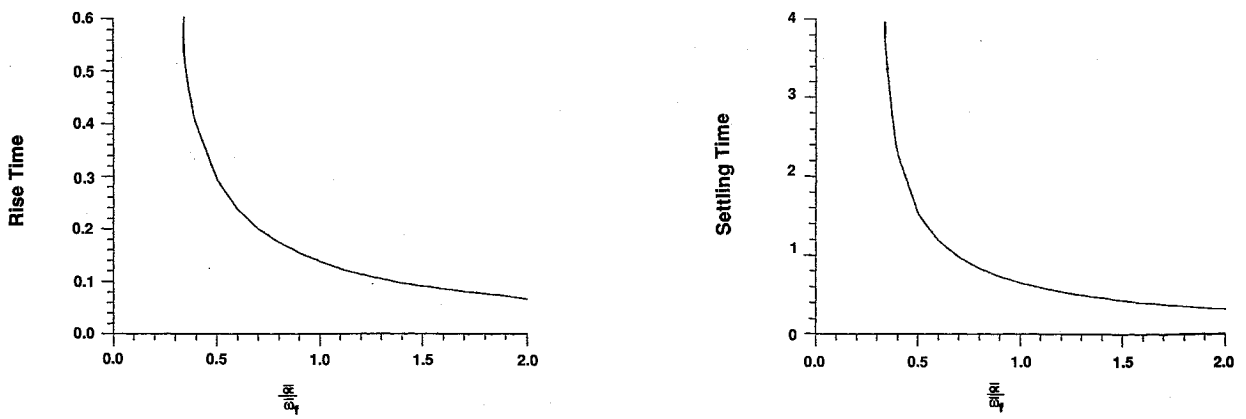

Fig. 3 Rise time and settling time of $\bar{\Omega}_3$ for spin-up maneuvering using a step function as the angular velocity for the shadow beam.

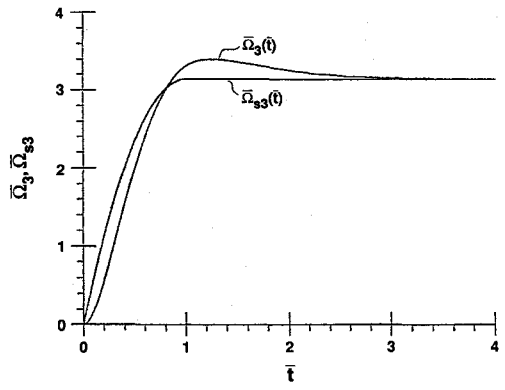

Fig. 4 Angular velocities for spin-up maneuvers using an optimal profile for the shadow beam.

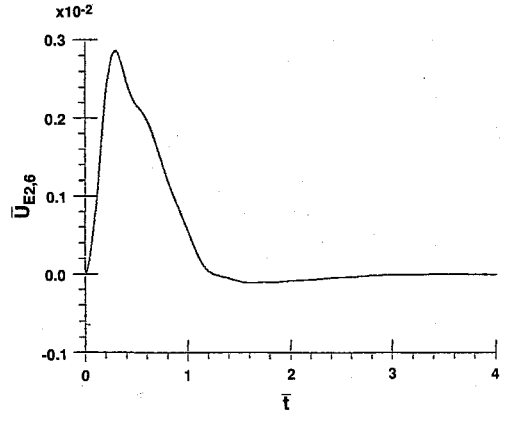

Fig. 5 Elastic deflection at the tip for spin-up maneuvers using an optimal profile for the shadow beam.

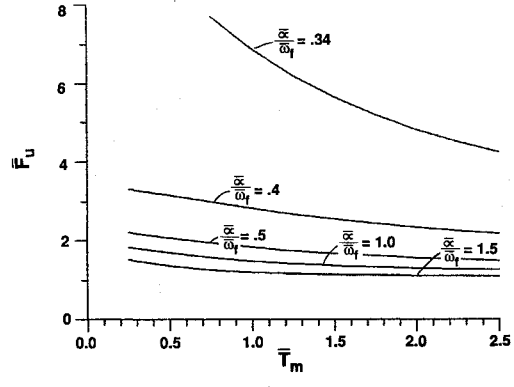

Fig. 6 Fuel vs maneuver time for spin-up maneuvers using an optimal profile for the shadow beam.

section, the shadow coordinates follow the path associated with the minimum fuel rest-to-spin maneuver for rigid bodies. For spin-up about the $\hat{b}_3$ axis, when $0 \le \bar{t} \le \bar{T}_m$, the shadow coordinates are given by

$$\bar{\Omega}_{s1}(\bar{t}) = 0, \quad \bar{\Omega}_{s2}(\bar{t}) = 0, \quad \bar{\Omega}_{s3}(\bar{t}) = \bar{\Omega}_m[2\bar{t} - (\bar{t}^2/\bar{T}_m)] \tag{13}$$

with

$\bar{T}_m$ = nondimensional final spin-up maneuver time
$\bar{\Omega}_m$ = nondimensional final angular velocity for spin up

The nondimensional fuel function is defined as

$$\bar{F}u = \int_0^{\infty} \sum_{r=1}^{6} |\bar{f}_{2r}(\bar{t})| \, d\bar{t} \tag{14}$$

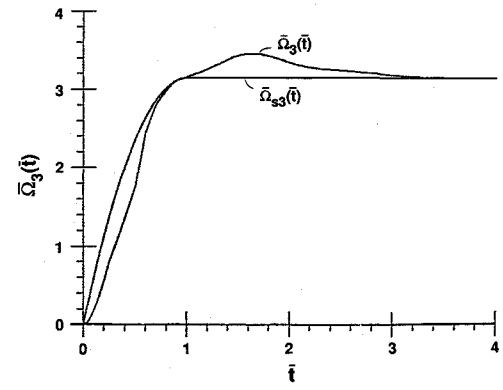

Fig. 7 Angular velocities for spin-up maneuvers using an optimal profile for the shadow beam with shut-down and explosive failures.

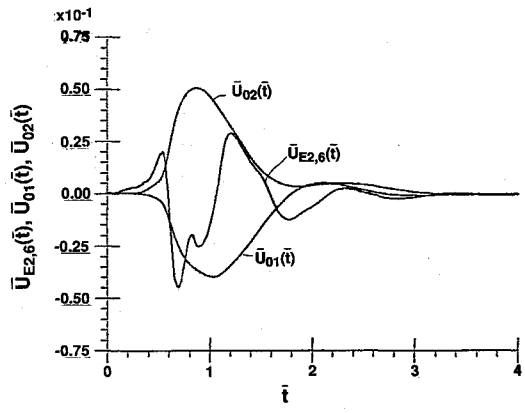

Fig. 8 Elastic deflection at the tip and inertial displacements of the mass center for spin-up maneuvers using an optimal profile for the shadow beam with shut-down and explosive failures.

We now let the control damping rate and the steady-state spin rate be identical to one-half the lowest natural frequency. The shadow coordinates reach the spin rate in one fundamental period. Figure 4 shows the angular velocity in the $\hat{b}_3$ direction of both the actual beam and the shadow beam. The elastic deflections at the tip are shown in Fig. 5. The control variables that spin up the beam are the control damping rate and the final spin-up maneuver time for which comparisons are made on the basis of the fuel function given in Eq. (14). Figure 6 shows the fuel as a function of maneuver time for different control damping rates normalized by the fundamental frequency. Note that higher damping rates reduce fuel because the beam follows the optimal path more closely. Also higher damping rates reduce structural vibration during the maneuver so that less fuel is expended to suppress vibration. Indeed, maneuvers are carried out more efficiently when structural vibration is not excited.

C. Multiple Actuator Failures

The spin-up maneuver described earlier is repeated here in the presence of multiple actuator failures. The first actuator (at $\bar{x}_1 = -0.5$) undergoes a shut-down failure and is turned off at $\bar{t} = \frac{1}{4}\bar{T}_m = \frac{1}{4}$. At $\bar{t} = \frac{1}{2}$, the fourth actuator (at $\bar{x}_4 = 0.1$) undergoes an explosive failure and is pulsed at a magnitude of $\bar{f}_{2,4} = 3$ for a period of time $\bar{t} = 1/10$ and then turned off. Note that the magnitude of the pulse is 20 times greater than the maximum acuator force associated with the same spin-up maneuver in the absence of failures. Figure 7 shows the angular velocities of the actual beam and the shadow beam. The shut-down failure and the explosive failure and the explosive failure cause the mass center to drift and cause the elastic deflections to increase as shown in Fig. 8. The spin-up maneuver, in the presence of these actuator failures,

successfully spins up the beam, suppresses the induced vibration, and eliminates the drift of the mass center.

D. Lag Compensation

In Sec. III.B., the shadow coordinates followed an optimal profile throughout the manuever. We also note that the angular velocity of the beam lagged the optimal angular velocity and that the lag decreased as the control damping rate increased. Here, we compensate for the lag by computing shadow coordinates that allow the beam to follow the optimal profile. Toward this end, using the equations of motion (8) and the control law [Eq. (11)], and assuming small angles between the floating and shadow coordinates, we obtain the closed-loop equations describing rotations about $\hat{b}_3$ as

$$\bar{\Omega}_3' = 2\bar{\alpha}\bar{I}_c(\bar{\Omega}_3 - \bar{\Omega}_{s3}) - \bar{\alpha}^2\bar{I}_c(\theta_3 - \theta_{s3}) \tag{15}$$

in which

$$\bar{\Omega}_3 = \theta_3', \quad \bar{\Omega}_{s3} = \theta_{s3}'$$

with

$$\bar{I}_c = \left(\sum_{r=1}^{6} \bar{m}_r\bar{x}_r^2\right)\Big/ I_3 \qquad \text{(nondimensional control moment of inertia)}$$

Letting $\bar{\Omega}_3$ be identical to the optimal profile [Eq. (13)], carrying out a differentiation and an integration to obtain Ω_3' and θ_3, respectively, and substituting the result into Eq. (15), we obtain the angular velocity of the shadow coordinates with lag compensation

$$\bar{\Omega}_{s3}(\bar{t}) = \frac{\bar{\Omega}_m}{\bar{T}_m^2}(2\bar{T}_m - \bar{t}^2) - \frac{2\bar{\Omega}_m}{\bar{\alpha}^2\bar{T}_m^2\bar{I}_c} + \frac{\bar{\Omega}_m}{\bar{\alpha}^2\bar{T}_m\bar{I}_c}(\bar{\alpha}\bar{T}_m + 2)e^{-\bar{\alpha}\bar{t}/2}$$

$$\bar{\Omega}_{s1} = 0, \quad \Omega_{s2} = 0, \quad \bar{t} \le \bar{T}_m; \quad \bar{\Omega}_{s3}(t) = \bar{\Omega}_m, \quad \bar{t} > T_m \tag{16}$$

Figure 9 shows the desired angular velocity of the beam $\bar{\Omega}_{s3}$ [Eq. (13)], the actual beam angular velocity $\bar{\Omega}_3$, and the shadow beam angular velocity $\bar{\Omega}_{s3}$ [Eq. (16)]. As shown, the actual beam closely follows the optimal profile with lag compensation. The difference between the angular velocity of the beam $\bar{\Omega}_3$ and the desired angular velocity $\bar{\Omega}_{s3}$ [Eq. (13)] is due to a small angle approximation made between the floating and shadow coordinates [Eq. (15)]. Figure 10 shows changes in fuel with respect to the maneuver time for several damping rates. Note that the fuel decreases with the introduction of lag compensation since the optimal profile is more closely followed.

IV. Decentralized Feedback Rest-to-Rest Maneuvers

A. In-Plane 180-deg Maneuver

We select shadow coordinates indentical to the body-fixed coordinates associated with a minimum fuel 180-deg rest-to-rest maneuver of a rigid body with lag compensation. With the introduction of the lag compensation, the beam undergoes the indicated minimum fuel maneuver. Assuming a small angle approximation between the floating and shadow coordinates, the angular velocities of the shadow coordinates with lag compensation become

$$\bar{\Omega}_{s3} = \frac{6\pi}{\bar{T}_m^3}(\bar{T}_m - \bar{t})\bar{t} + \left\{-\frac{\pi}{3\bar{\alpha}^2\bar{I}_c\bar{T}_m^3} + \frac{\pi}{12\bar{\alpha}^2\bar{I}_c\bar{T}_m^3}(\bar{\alpha}\bar{T}_m + 4)e^{-\bar{\alpha}\bar{t}/2}\right\}$$

$$\Omega_{s1} = \bar{\Omega}_{s2} = 0, \quad t \le T_m, \quad \theta_{s3} = \pi, \quad \bar{\Omega}_{s3} = 0, \quad \bar{t} > \bar{T}_m \tag{17}$$

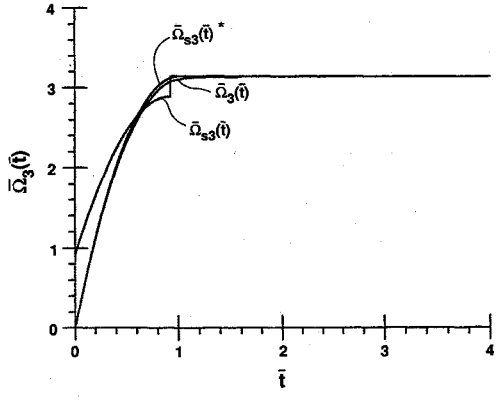

Fig. 9 Angular velocities for spin-up maneuvers using a lag compensating shadow beam [the desired angular velocity of the actual beam; using Eq. (13)].

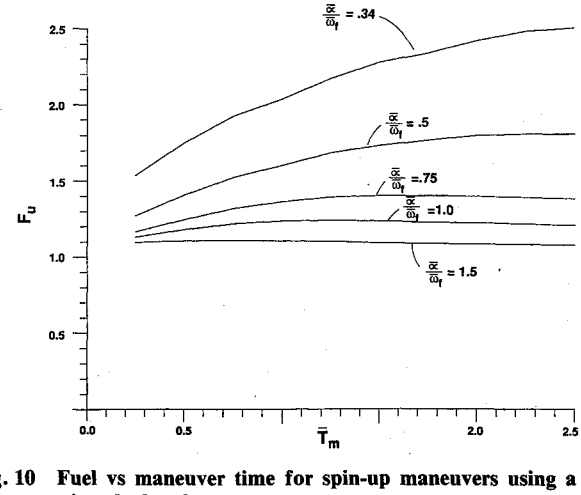

Fig. 10 Fuel vs maneuver time for spin-up maneuvers using a lag compensating shadow beam.

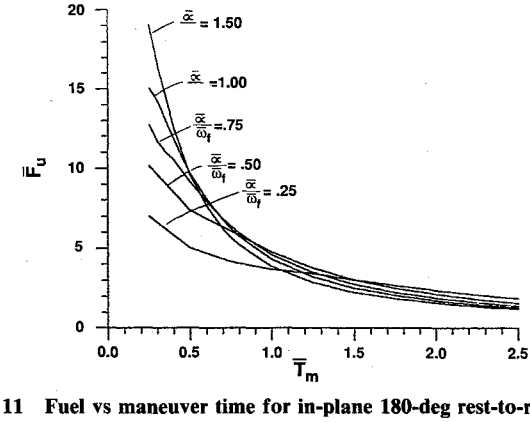

Fig. 11 Fuel vs maneuver time for in-plane 180-deg rest-to-rest maneuvers using an optimal profile for the shadow beam.

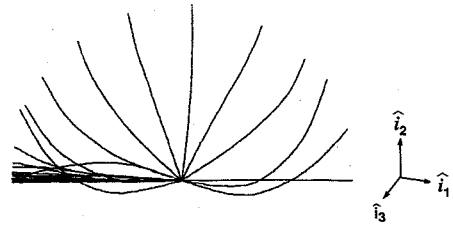

Fig. 12 Time lapses of the beam's right half with the elastic deflections magnified by 15 and with one-tenth the fundamental period time lapses.

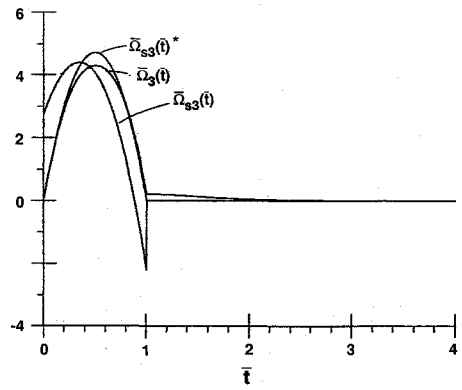

Fig. 13 Angular velocities for in-plane 180-deg rest-to-rest maneuvers using a lag compensating shadow beam [the desired angular velocity of the actual beam; using Eq. (17) without the brackets].

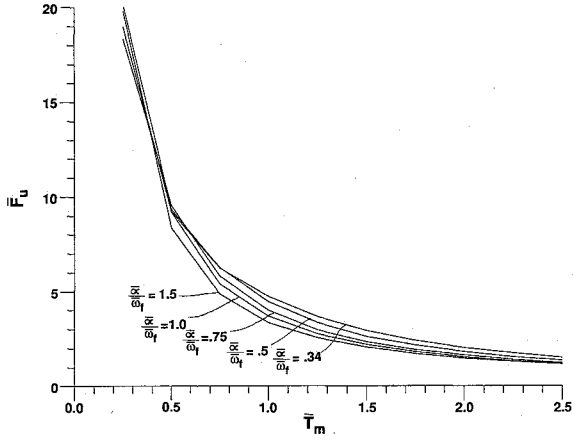

Fig. 14 Fuel vs maneuver time for in-plane 180-deg rest-to-rest maneuvers using a lag compensating shadow beam.

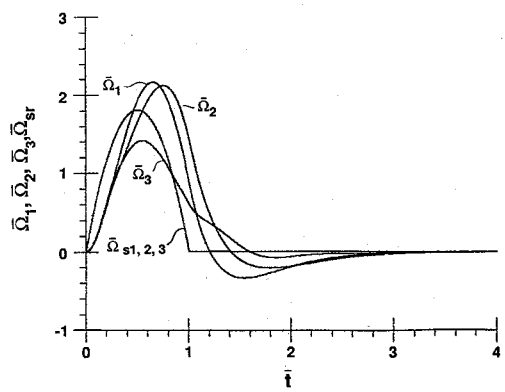

Fig. 15 Angular velocities for out-of-plane rest-to-rest maneuvers.

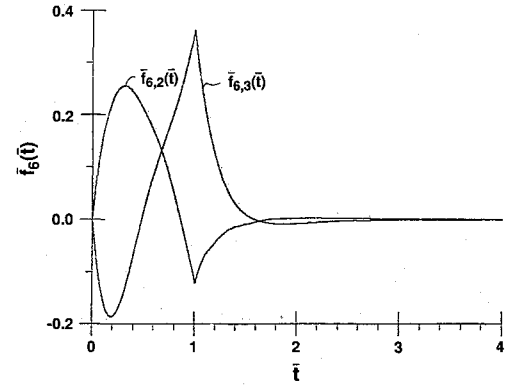

Fig. 16 Control forces in the $\hat{b}_2$ and $\hat{b}_3$ directions at the tip for out-of-plane rest-to-rest maneuvers.

in which the first term of $\bar{\Omega}_{s3}$ in Eq. (17) represents the indicated minimum fuel maneuver and the second and third terms (enclosed in brackets) are lag compensating terms. First, neglecting the lag compensating terms in the brackets in Eq. (17), fuel is expressed as a function of the maneuver times (in periods of the fundamental frequency) for several control damping rates normalized by the fundamental frequency (see Fig. 11). At the lower damping rates and for more rapid maneuvers, the fuel is lower because of the lag in the control law. The lag has the effect of increasing the maneuver time T_m. At the slower maneuver times, the higher damping rates require less fuel because they allow the beam to rotate closer to the optimal profile. Next, Fig. 12 shows a time lapse of the right half of the beam. Figure 13 shows the angular velocities of the actual beam $\bar{\Omega}_3$, the shadow beam $\bar{\Omega}_{s3}$ [Eq. (17)], and the desired angular velocities of the beam $\bar{\Omega}_{s3}$ [Eq. (17) without the brackets]. As shown, the actual beam closely follows the desired optimal profile, although not exactly, due to a small angle approximation made between the floating the shadow coordinates. Figure 14 shows changes in fuel with respect to the maneuver time for several damping rates. Note that the fuel consumed is insensitive to changes in the damping rates since with the introduction of lag compensation, the beam more closely follows the desired optimal profile.

B. Out-of-Plane 120-deg Single-Axis Maneuver

Consider the out-of-plane rest-to-rest maneuver about the single rotation axis $\hat{l} = l_1\hat{b}_1 + l_2\hat{b}_2 + l_3\hat{b}_3$ in which $l_1 = l_2 = l_3 = \sqrt{3}/3$. The beam rotates an angle $\Phi = 120$ deg about $\hat{l}$. Note that the term $(\theta_1 - \theta_{s1})$ in Eq. (11) is determined from the (2,3) entry of the coordinate transformation matrix between the shadow coordinates and the floating coordinates. We let the shadow coordinates rotate at the angular velocities

$$\bar{\Omega}_{sr}(\bar{t}) = l_r \frac{6\Phi}{\bar{T}_m^3}(T_m - \bar{t})\bar{t}, \qquad r = 1,2,3 \tag{18}$$

with

$l_r = r$th component of single rotation axis
Φ = single angle of rotation

Whereas the shadow coordinates given in Eq. (18) would be associated with a minimum fuel maneuver for rigid bodies had the rotation axis $\hat{l}$ been a principal axis; the rotation axis considered here is not a principal axis, therefore, the shadow spacecraft considered here follows a nonoptimal profile. The control damping rate was chosen as one-half the lowest natural frequency. Figure 15 shows the angular velocities $\bar{\Omega}_1$, $\bar{\Omega}_2$, and $\bar{\Omega}_3$ as compared with $\bar{\Omega}_{sr}$, $r = 1,2,3$. Figure 16 shows the actuator forces at the tip of the beam in the $\hat{b}_2$ and $\hat{b}_3$ directions. Note that the force in the $\hat{b}_3$ direction $[\bar{f}_{36}(\bar{t})]$ effects only a rigid-body motion, whereas the force in the $\hat{b}_2$ direction $[\bar{f}_{26}(t)]$ controls rigid-body motion and suppresses vibration.

V. Summary

A novel approach to maneuver of flexible spacecraft was described in which spacecraft motion relative to the motion of a shadow spacecraft is suppressed using a decentralized feedback control. In contrast with techniques requiring the solution of high-dimensional two-point boundary-value problems, this approach leads to near-optimal solutions using an algorithm well suited for in-space implementation.

For both rest-to-spin and rest-to-rest maneuvers, lag compensating shadow spacecraft were developed to enable the

spacecraft to follow optimal profiles. Without lag compensation, it was verified that the fuel to carry out maneuvers increased with decreasing decay rates as a result of the increase in lag between the spacecraft and its shadow. However, with the introduction of lag compensation, the associated fuel decreased with decreasing decay rates, as is the case in vibration-suppression problems. This indicates that the lag compensating decentralized feedback maneuvers are near-optimal. Furthermore, a high level of system level reliability was achieved by suppressing the relative motion between the actual spacecraft and its shadow using decentralized feedback in which the relative motion must be measured in inertial coordinates. As an illustration, a spacecraft maneuver was successfully performed in the presence of both a shut-down actuator failure and an explosive actuator failure.

References

[1]Junkins, J. L. and Thompson, R. C., "An Asymptotic Perturbation Method for Nonlinear Optimal Control Problems," *Journal of Guidance, Control, and Dynamics*, Vol. 9, Sept.-Oct. 1986, pp. 391-396.

[2]Silverberg, L., "Uniform Damping Control of Spacecraft," *Journal of Guidance, Control, and Dynamics*, Vol. 9, March-April 1986, pp. 221-227.

[3]Meriovitch, L., *Analytical Methods in Vibrations*, McMillan, New York, 1967.

[4]Canavin, J. R. and Liken, P. W., "Floating Reference Frames for Flexible Spacecraft," *Journal of Spacecraft and Rockets*, Vol. 14, Dec. 1977, pp. 724-732.

[5]Silverberg, L. and Park, S., "The Interactions Between Rigid-Body and Flexible-Body Motions in Maneuvering Spacecraft," *Journal of Guidance, Control, and Dynamics*, Vol. 13, No. 1, 1990, pp. 73-81.